Cohesive, structural, and electronic properties of Fe-Si compounds

E. G. Moroni
Institut für Theoretische Physik, Technische Universität Wien, Wiedner Hauptstrasse 8-10/136, A-1040 Vienna, Austria and Center for Computational Material Science, A-1060 Vienna, Austria

W. Wolf
Institut für Physikalische Chemie, Universität Wien, Liechtensteinstrasse 22A, A-1090 Vienna, Austria

J. Hafner
Institut für Theoretische Physik, Technische Universität Wien, Wiedner Haupstrasse 8-10/136, A-1040 Vienna, Austria and Center for Computational Material Science, A-1060 Vienna, Austria

R. Podloucky
Institut für Physikalische Chemie, Universität Wien, Liechtensteinstrasse 22A, A-1090 Vienna, Austria and Center for Computational Material Science, A-1060 Vienna, Austria

(Received 1 December 1998)

Phase stability, structural, and electronic properties of iron silicides in the Fe_3Si, FeSi, and $FeSi_2$ compositions are investigated by first-principle density-functional calculations based on ultrasoft pseudopotentials and all-electron methods. Structural stabilization versus spin-polarization effects are discussed at the Fe_3Si composition, while for ϵ-FeSi and β-$FeSi_2$ we investigate their structural properties and the corresponding semiconducting band properties. All the computed results are analyzed and compared to available experimental data. The stability of the bulk phases, the lattice parameters, the cohesive energies and magnetic properties are found to be in good agreement with experiment when using the generalized gradient approximations for the exchange-correlation functional. Density-functional calculations are unable to account for the small bulk modulus of ϵ-FeSi despite that the computed lattice constant and internal atomic positions coincide with the experimental results. Both full-potential and ultrasoft-pseudopotential methods confirm for β-$FeSi_2$ the indirect nature of the fundamental gap, which is attributed to a transition between Y to $0.6\times\Lambda$ being 30% smaller than the experimental gap. Ultrasoft pseudopotential calculations of Fe-Si magnetic phases and of various nonequilibrium metallic phases at the FeSi and $FeSi_2$ composition are presented. These calculations provide *ab initio* information concerning the stabilization of metallic pseudomorphic phases via high pressures or epitaxy. [S0163-1829(99)05419-3]

I. INTRODUCTION

In the past decade, the aim of creating suitable metal-semiconductor contacts (Schottky junctions)[1] has motivated many experimental investigations of the stability of silicides when grown epitaxially on Si. The fluorite structure is grown on silicon with excellent quality for metallic $CoSi_2$ and $NiSi_2$ films.[2] Considerable complications occur for $FeSi_2$ films mainly because of the poor geometrical matching of the orthorhombic β phase onto the Si(111) and Si(100) substrates.[3] Due to this unfavourable geometrical relationship, various Fe silicide cubic structures, which are related to defected CsCl ($B2$) lattices are formed as thin films and have been experimentally characterized during the last few years.[4] In contrast to the semiconducting β phase, the epitaxially grown cubic phases exhibit metallic conductivity.

More recently, studies have been devoted to the understanding of the magnetic properties of Fe/Si, Fe/Fe-Si, and Fe-Si/Fe_3Si multilayers,[5] mainly in relation to possible applications in the field of giant magnetoresistence. Different to metal/metal multilayers, the exchange coupling properties of Fe/Si multilayers with semiconducting spacers are still unclear.[6] This is due, in particular, to an insufficient understanding of the relation between the formation of metallic silicides in the interlayer and the antiferromagnetic coupling. Interest on magnetism of iron silicides is also stimulated by the research on transition-metal silicon compounds exhibiting both ferromagnetic ordering and high-quality epitaxial growth on Si. Evidence has been recently found for the formation of a ferromagnetic iron silicide at the Fe/Si(100) interface and its magnetic properties have been studied by spin- and angle-resolved photoemission.[7] Finally, Fe-Si-based materials are interesting because of the technological issues of integrating on a unique device both magnetic, optical, and electronic components.

A few theoretical studies have been undertaken to calculate the electronic structure and bonding properties of a few selected bulk phases of iron silicides. The electronic structure and magnetic properties of Fe_3Si and related ternary systems have been investigated by Kudrnovsky, Christensen, and Andersen.[8] The compound Fe_3Si exists over a wide composition range with the DO_3 structure and exhibits ferromagnetic ordering. Upon heating, it transforms to a $B2$ structure, and prior to melting to a disordered structure. Interest in this material is motivated by its intriguing magnetic properties and because of the site-occupation preference of

substitutional transition-metal impurities in this material.[9]

The structure of Fe_3Si is characterized by maintaining almost the same interatomic Fe nearest-neighbor (NN) distance as in bcc Fe and in pseudomorphic $B2$ FeSi. The small misfit and the similar epitaxial behavior of these structures are relevant factors in the stabilization of $B2$ FeSi films on the $Fe_3Si(100)$ surface, mainly because of the preferential segregation of Si to the surface.[10] This may lead to a more efficient fabrication of Fe/FeSi/Fe heterostructures.

At the 1:1 composition bulk FeSi assumes the cubic $B20$ structure (ϵ-FeSi). At high temperatures, it shows anomalous magnetic properties, with a maximum of the susceptibility at 500 K, while at low temperature the peculiar feature is a very small band gap of about 50 meV. The semiconducting properties have been studied theoretically by band-structure calculations by Mattheiss and Hamann.[11] The $B20$ structure can be seen as a distortion of the rocksalt structure ($B1$). The small gap in the middle of the $3d$ bands of ϵ-FeSi can be traced back to the pseudogap present in this unstable phase.[11] However, a sufficient number of electronic excitations occurs across the gap even at moderate temperatures of $T \approx 300$ K so that ϵ-FeSi becomes a poor metal. The anomalous thermal magnetic properties have been explained using spin-fluctuations models by Jarlborg[12] and using a Kondo insulator description by Mandrus *et al.*,[13] while Fu, Krijn, and Doniach[14] investigated the optical properties of FeSi indicating large discrepancies between band theory and measured data.

For the 1:2 composition the band structure and semiconducting properties of β-$FeSi_2$ have been investigated by Christensen[15] and Eppenga.[16] Comparison between computed and experimental optical properties have been presented by Antonov *et al.*,[17] which claim excellent agreement between measurement and the calculations. Soft-x-ray emission and -absorption spectra of β-$FeSi_2$ and of the high-temperature bulk stable phase (α-$FeSi_2$) have been studied by Eisebitt *et al.*[18] The electronic structure of the epitaxially stabilized $B2$ FeSi and γ-$FeSi_2$ cubic structure have been described by Mäder, von Känel, and Baldereschi[19] by an *ab initio* method. The structural relation between these pseudomorphic phases and the ground-state structure have been investigated using a tight-binding molecular-dynamic method by Miglio *et al.*[20]

The manifold of new applications of Fe-Si bulk materials, thin films, and epitaxial compounds and the scarcing of *ab initio* studies of the electronic and structural effects of bulk-stable and epitaxially stabilized iron silicides compounds motivates our investigation. This work will be split into two papers. In this first paper, we present an *ab initio* study of the electronic structure and total energy properties of the bulk-stable and other unstable structures of Fe_3Si, FeSi and $FeSi_2$ compounds. In a second paper, we will present the strain and epitaxial properties of selected Fe-Si compounds.[21] The numerical calculations are performed using a plane-wave basis set and ultrasoft pseudopotential (USPP), as well as full potential all-electron methods. Here, the USPP are used to compute structural and atomic relaxations and to study the complex interplay of the structural and electronic degree of freedom from magnetic (Fe_3Si) to semiconductor (ϵ-FeSi and β-$FeSi_2$), and defected Fe-Si metallic phases ($FeSi_{1+x}$ and γ-$FeSi_2$). No attempts have been made previously to use pseudopotential techniques to study structural properties in Fe-Si systems because of the difficulties to describe localized and magnetic $3d$ states.

II. COMPUTATIONAL ASPECTS

A. Methods and techniques

Most calculations presented here have been done using the Vienna *ab initio* simulation package[22] (VASP) with ultrasoft pseudopotential. For the exchange-correlation functional both the local-spin-density (LSD) approximation with the parametrization of Perdew-Zunger[23] and the generalized gradient approximation (GGA) of Perdew and Wang[24] have been used. For intermediate spin polarizations the interpolation formula of von Barth and Hedin[25] are applied. The approach of White and Bird[26] has been used for the computation of GGA exchange-correlation potentials and extended to treat spin-polarized states.[34] VASP is a plane-wave code based on ultrasoft pseudopotentials, and uses iterative strategies based on residual minimization[27] and preconditioned conjugate-gradient techniques for the diagonalization of the Kohn-Sham Hamiltonian. A detailed description of VASP and its algorithm can be found in Ref. 22.

The full-potential linearized augmented plane-wave method[28] (FLAPW) within the LSD approximation, has been used to provide reliable all-electron reference results for assessing the quality of the ultrasoft pseudopotentials.

Brillouin-zone integrations are performed on a grid of Monkhorst-Pack special points[29] by using different schemes. The linear tetrahedron method including the corrections of Blöchl[30] has been chosen to improve the convergence of total energy with respect to the number of k points. Smearing methods[31] with Methfessel and Paxton[32] broadening function are used when exact forces are required.

For comparison of different structures and compositions it is necessary to care about the convergence of total energy and equilibrium properties calculations. The convergence of these integration methods, with respect to the number of k points has been tested for all structures using both LSD and GGA functionals. Here, we give some results for the metallic pseudomorphic phase of FeSi with the $B2$ structure characterized by a pseudogap below and a very sharp peak just above the Fermi level. Its total energy has been computed using sets of 220, 120, 84, 56, 35, 10, and 4 k points in the irreducible wedge of the Brillouin zone. The total energy is converged within differences smaller than 0.001 eV when using 84 k points or more, while errors of 0.002, 0.004, 0.016, and 0.135 eV arise for the 56, 35, 10, and 4 k point sets, respectively. A similar fast convergence is also found for other related quantities, such as the equilibrium ground-state properties. For $B2$ FeSi, the computed LSD equilibrium volume and bulk modulus differ by 0.002 $Å^3$ and 10 Kbar when using 120 and 220 k points, respectively.

When using VASP, the electron-ion interaction is described using ultrasoft pseudopotential (USPP).[33,34] Fe USPP has been generated in the nonmagnetic $4s^1 3d^7$ atomic configuration, with cutoff radii of 2.2, 2.45, and 2.45 a.u. for, respectively the $4s$, $4p$, and $3d$ wave components. The logaritmic derivatives of the pseudowave function are very accurate not only for the $l=0,1,2$ components but also for the unoccupied $l=3$ (f states) over a wide range of energies (see

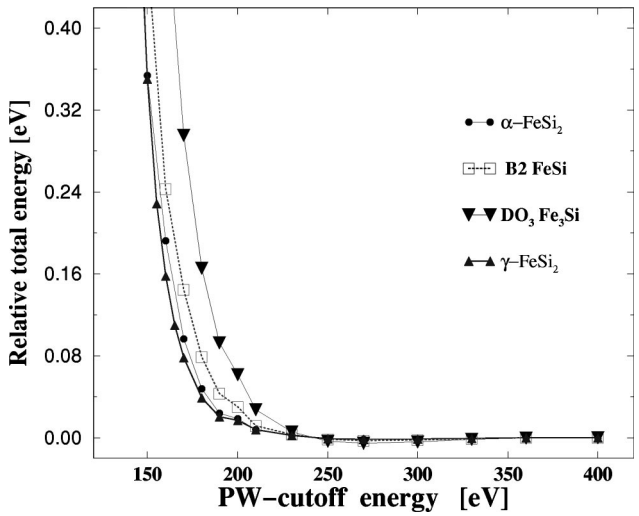

FIG. 1. Calculated total energy per atom for α-$FeSi_2$, $B2$ FeSi, DO_3 Fe_3Si, and γ-$FeSi_2$ versus the cutoff energy of the plane-wave basis set. The total energy are referenced to the total energy obtained using a cutoff energy of 400 eV.

Fig. 1 in Ref. 34). The screened all-electron potential was truncated at $r_{\mathrm{loc}}=1.7$ a.u. and chosen as the local potential. To describe the valence core energy interaction and spin-polarization effects accurately the nonlinear partial core correction scheme proposed by Louie, Froyen, and Cohen[35] has been used.

For Si, the pseudopotential has been generated in the $3s^2 3p^2$ atomic configuration. In this case, we used an ultrasoft pseudopotential with two reference energies for the $3s$ and $3p$ states and a norm-conserving pseudopotential with a single reference energy for the $3d$ component. As local potential we have used the $3d$ pseudopotential.

The transferability of USPP and the plane-wave expansion of the US pseudowave function are optimized at an energy cutoff of 18 Ry. For all studied Fe-Si structures the relative total energy is converged to within 1 meV for a cutoff energy of the plane-wave basis set of 250 eV or higher. Figure 1 illustrates the fast convergence of the relative total energy versus cutoff energy (E_{cut}) for four different Fe-Si compounds. The convergence is fast and independent of the crystal environment. A reduction of E_{cut} influences strongly the accuracy of the computed structural properties and the differences of the cohesive energies increases rapidly. The convergence of the magnetic moment of Fe and Si in Fe_3Si is confirmed by Fig. 2, which presents the ratio of magnetic moments computed at various plane-wave cutoff energies (from 180 to 400 eV) with respect to the reference magnetic moment computed at a cutoff energy of 400 eV.

We have also generated an USPP for Fe in the $3p^6 4s^1 3d^7$ nonmagnetic configuration including the $3p$ semicore states as valence states. In this case the cutoff radii of the pseudowave function were reduced to 1.9 a.u. and a larger cutoff energy of 320 eV is required for converged results. As for bcc Fe,[34] also for Fe_3Si when we use the USPP without semicore states GGA overestimates the magnetic moment by about 0.1 μ_B and the magnetic energy of about 40 meV per atom. As shown in Table II these small magnetic differences

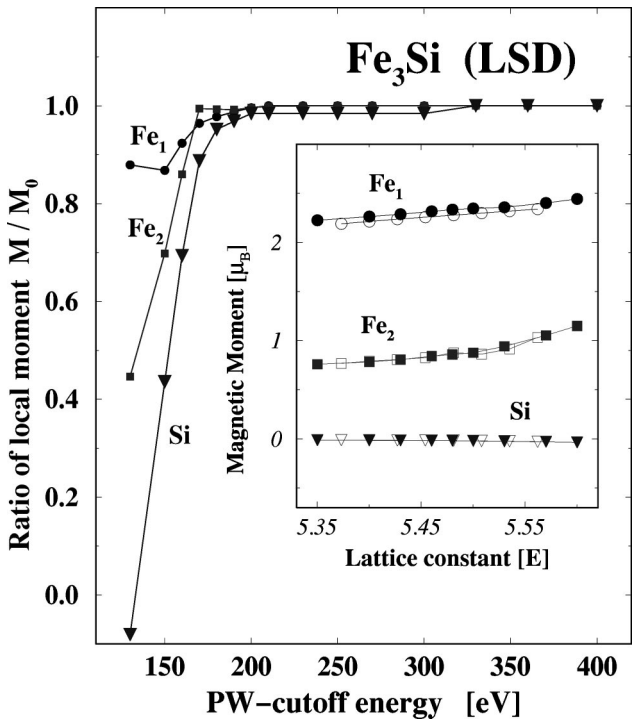

FIG. 2. Convergence of magnetic properties of Fe_3Si versus the cutoff energy of the plane-wave basis set. For E_{cut} varying from 120 to 400 eV we show the ratio of the computed Fe and Si magnetic moments with respect to the reference moments evaluated for a cutoff energy of 400 eV. In the inset are compared the calculated local moments as a function of lattice constants using LSD FLAPW (open symbol) and LSD USPP (filled symbol).

affect the corresponding equilibrium bulk properties. More details concerning the applied USPP are given in Ref. 34.

B. Comparison of USPP and FLAPW results

In this section, we describe briefly the principal features of the used methods and we present the transferability of USPP for describing the ground-state and electronic properties of several crystal structures for the Fe_3Si, FeSi, $FeSi_2$ composition, along with pure Fe and Si. A compilation of all the crystal structures covered in this study is presented in Table I. The total energy of the known stable crystal structures and of some selected metastable and unstable Fe-Si compounds are computed as a function of volumes using both *ab initio* methods described above. From Murnaghan least-squares fits[38] of the total energy versus volume we obtain the equilibrium volume V_0, the bulk modulus B_0 and its pressure derivative $B_0'=(\partial B/\partial P)_{P=0}$.

Table II compares the USPP and FLAPW results for the total energy and magnetic properties of various Fe-Si compounds. An excellent agreement is obtained for the equilibrium and structural properties of nonmagnetic FeSi and $FeSi_2$ selected compounds. For the spin-polarized Fe_3Si, the computed equilibrium lattice constants differs of about 0.3% (0.02 Å) and the bulk modulus differs of about 10%. As shown in Fig. 2 and Table II the magnetic moments on the Fe and Si sites in Fe_3Si agree within 0.1 μ_B. A reduction in magnetic moments and a related increase in the bulk modulus is obtained by including the full relaxation of $3p$ semi-

TABLE I. List of structures considered in this study. See Ref. 36 for Pearson symbol.

Material	Proto-type	Struktur-bericht	Pearson symbol	Space group	Space group number
Fe	W	$A2$	$cI2$	$Im\bar{3}m$	229
	Cu	$A1$	$cF4$	$Fm\bar{3}m$	225
Fe_3Si	BiF_3	$D0_3$	$cF16$	$Fm\bar{3}m$	225
FeSi	FeSi	$B20$	$cP8$	$P2_13$	198
	ClCs	$B2$	$cP2$	$Pm\bar{3}m$	221
	MnP	$B31$	$oP8$	$Pnma$	62
	CoSn	$B35$	$hP6$	$P6/mmm$	191
	NaCl	$B1$	$cF8$	$Fm\bar{3}m$	225
β-$FeSi_2$	$FeSi_2$		$oC48$	$Cmca$	64
α-$FeSi_2$	$FeSi_2$		$tP3$	$P4/mmm$	123
γ-$FeSi_2$	CaF_2	$C1$	$cF12$	$Fm\bar{3}m$	225
Si	C	$A4$	$cF8$	$Fd\bar{3}m$	227

core states in the USPP.[34] Previous LSD linear muffin-tin orbital[8] and augmented-spherical-waves[39] calculations lead to Fe moment of 1.2-1.4 μ_B and of $\approx$2.5 μ_B for the two different Fe sites in Fe_3Si. We found smaller magnetic moments of about 0.8-0.9 μ_B for the Fe atom, which has 4 Fe and 4 Si NN and $\approx$2.3 μ_B for the eightfold coordinated Fe atoms. These differences are mainly related to the nonspherical terms of the potentials and to different treatements of the interstitial region. Using full-potential methods the magnetic moments are reduced by about 0.4 μ_B for the fourfold coordinated Fe atoms.

The transferability of USPP is confirmed also for density of states and band-structure properties. In Fig. 3 we present the total density of states (DOS) of selected bulk-stable Fe-Si compounds with the Fermi level taken as the zero of energy. These DOS obtained from USPP are equal with the DOS obtained by FLAPW. For Fe and Fe_3Si we plot the spin-polarized DOS for majority and minority spin. The total integrated areas of the DOS up to the Fermi level in Fig. 3 are

TABLE II. Comparison of LSD and GGA ultrasoft pseudopotential (USPP) with LSD all-electron FLAPW calculations and experiment for equilibrium and magnetic properties of Fe-Si compounds. For $A2$ Fe and DO_3 Fe_3Si, are compared the equilibrium lattice constant a, the bulk modulus B, the local magnetic moment M_i, and the respective magnetic energy ΔE_m. For $B2$ and $B20$ FeSi, α- and γ-$FeSi_2$ and pure Si, are compared the equilibrium lattice constant a, the bulk modulus B. At the 1:2 stoichiometry we compare also the total energy difference between the γ- and the α-$FeSi_2$ structure, and the internal Si atomic coordinate z in α-$FeSi_2$. For the Fe atom the GGA USPP $ps1$ was generated for the $4s^13d^7$ and $ps2$ for the $3p^64s^13d^7$ atomic configurations (i.e., treating the $3p$ electrons as valence electrons).

			LSD		GGA		
		Units	FLAPW	USPP	$ps1$	$ps2$	EXP
Fe $A2$	a_{FM}	Å	2.76	2.76	2.86	2.87	2.87[a]
	a_{NM}	Å	2.70	2.70	2.79	2.78	
	B_{FM}	Mbar	2.38	2.35	1.55	1.66	1.683[a]
	ΔE_m	eV/at	0.25	0.30	0.55	0.49	
	M_{Fe}	μ_B	2.03	2.05	2.32	2.24	2.22[a]
Fe_3Si DO_3	a_{FM}	Å	5.47	5.49	5.63	5.63	5.65[b]
	a_{NM}	Å	5.44	5.45	5.55	5.55	
	B_{FM}	Mbar	2.67	2.47	1.97	2.14	
	B_{NM}	Mbar	3.02	2.93	2.48	2.50	
	ΔE_m	eV/f.u.	0.74	0.69	1.20	1.04	
	M_{Fe}	μ_B	2.27	2.34	2.61	2.55	2.2-2.4[c]
	M_{Fe}	μ_B	0.83	0.87	1.37	1.33	1.35[c]
	M_{Si}	μ_B	−0.02	−0.02	−0.06	−0.05	−0.07[c]
FeSi $B20$	a_{NM}	Å	4.41	4.38	4.46	4.47	4.489[b]
	B_{NM}	Mbar	2.55	2.57	2.23	2.24	1.1–1.3[e]
FeSi $B2$	a_{NM}	Å	2.72	2.72	2.77	2.77	2.77[d]
	B_{NM}	Mbar	2.70	2.63	2.21	2.23	2.22[d]
α-$FeSi_2$	a_{NM}	Å	2.66	2.66	2.71	2.71	2.69[b]
	c_{NM}	Å	5.08	5.08	5.14	5.14	5.134[b]
	B_{NM}	Mbar	2.13	2.06	1.72	1.75	
	z		0.272	0.272	0.273	0.273	0.28[b]
γ-$FeSi_2$	a_{NM}	Å	5.32	5.31	5.40	5.41	
	B_{NM}	Mbar	1.96	1.93	1.67	1.67	
	E_γ-E_α	eV/f.u.	0.32	0.30	0.36	0.33	
Si $A4$	a_{NM}	Å	5.41	5.40	5.46		5.43[a]
	B_{NM}	Mbar	0.99	0.95	0.87		0.988[a]

[a]Reference 37.
[b]Reference 36.
[c]Reference 9.
[d]Reference 4.
[e]Reference 43.

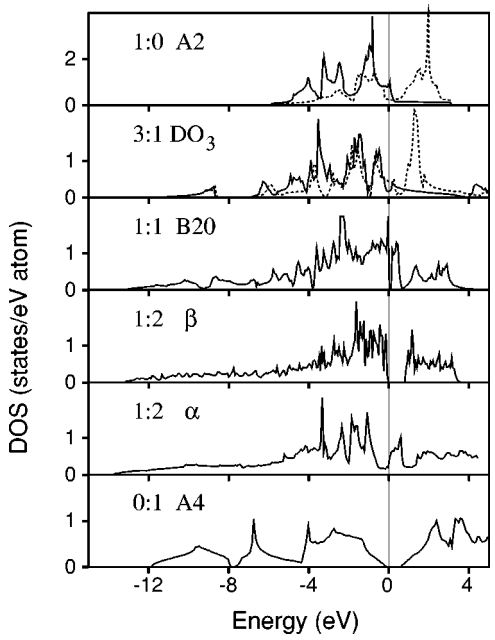

FIG. 3. Density of states for the six members of the Fe-Si series, identified by their stoichiometry and crystal structure type. The Fermi level is taken as the zero of energy.

8, 7, 6, 5.33, and 4 electrons for Fe, Fe_3Si, FeSi, $FeSi_2$, and Si, respectively. Along this series ϵ-FeSi with a very small optical gap separates Si and β-$FeSi_2$, which display semiconducting properties of different origin, from the metallic and ferromagnetically ordered Fe and Fe_3Si compounds.

To prove the transferability of USPP for band-structure results we present in Fig. 9 the band structure of β-$FeSi_2$ in the vicinity of the band gap as computed using USPP and FLAPW. The band structure was plotted with 245 k points along the high-symmetry lines of the base-centered orthorhombic Brillouin zone. The calculation is based on the experimental lattice parameters and the experimental atomic positions taken from Dusausoy *et al.*[40] The discrepancies between the two band-structure calculations are very small and do not influence the dispersions of the bands close to the gap. Related electronic properties will be discussed more in detail in Sec. III C 2 and compared with GGA results.

III. RESULTS AND DISCUSSION

A. LSD versus GGA for cohesive properties

The influence of gradient corrections to the local exchange-correlation functional is analyzed here for the total energy and magnetic properties of Fe-Si compounds using USPP and whenever possible compared to experimental measurements. Table III summarizes the computed equilibrium volume (per atom) V_0, the bulk modulus B_0, the heat of formation ΔH, and the cohesive energy E_{coh} using USPP calculations by comparing both the LSD and GGA functionals, along with the corresponding available experimental data. The cohesive energies E_{coh} are obtained by subtracting from the total energy of the solid at the equilibrium lattice constant the sum of the pseudoatom total energies, using the spin-polarized results for the Fe and Si pseudoatom. For isolated atoms the LSD and GGA atomic ground states are the spin-polarized configuration $3d^{6.2}4s^{1.8}$ for Fe and the $3s^2 3p^2$ for Si. The corresponding atomic spin energies are 2.82 and 0.62 eV/atom, respectively, by using LSD and of 3.15 and 0.76 eV/atom by using GGA. Note that LSD and GGA calculations for Fe predict the wrong atomic ground state (see Ref. 34). The heat of formation ΔH of the iron silicide series is evaluated with respect to the ground state of Fe (FM bcc) and Si (NM diamond).

Figure 4 shows the GGA heat of formation ΔH and the respective bulk modulus of the Fe-Si compounds as a function of composition. For all Fe-Si compound with 3:1, 1:1, and 1:2 stoichiometry we obtain the correct stable crystal structure, in good agreement with the experimental phase diagram. The available experimental ΔH values[41] for iron

TABLE III. Calculated equilibrium volume V_0, bulk modulus B_0, heat of formation ΔH, and cohesive energy E_{coh} for the iron silicides series. The LSD and GGA results are compared with experimental values.

Composition	Strukturbericht		V_0(Å^3/atom)			B_0 (Mbar)			ΔH (eV/atom)			E_{coh} (eV/atom)		
			LSD	GGA	exp	LSD	GGA	exp	LSD	GGA	exp	LSD	GGA	exp
Fe	$A2$	FM	10.54	11.73	11.79[a]	2.35	1.55	1.68[a]	0.00	0.00	0.00	6.47	5.15	4.28[a]
		NM	9.89	10.72		3.05	2.39		0.30	0.55				
	$A1$	NM	9.69	10.50		3.27	2.60		−0.04	0.24				
Fe_3Si	DO_3	FM	10.36	11.17	11.27[c]	2.42	1.99		−0.41	−0.28	−0.21[b]	6.59	5.30	
		NM	10.04	10.70		2.87	2.46		−0.22	0.03				
FeSi	$B20$	NM	10.50	11.12	11.24[c]	2.57	2.09	1.1–1.3[d]	−0.68	−0.42	−0.41[b]	6.58	5.33	
	$B2$	NM	10.02	10.63	10.63[e]	2.63	2.21	2.22[d]	−0.67	−0.38				
β-$FeSi_2$		NM	11.95	12.59	12.53[c]	2.09	1.82		−0.58	−0.37		6.30	5.20	
α-$FeSi_2$		NM	11.94	12.55	12.38[c]	2.06	1.72		−0.53	−0.31				
γ-$FeSi_2$	$C1$	NM	12.48	13.14		1.93	1.67		−0.41	−0.19				
Si	$A4$	NM	19.62	20.34	20.01[a]	0.94	0.87	0.988[a]	0.00	0.00	0.00	5.34	4.66	4.64[a]

[a]Reference 37.
[b]Reference 41.
[c]Reference 36.
[d]Reference 43.
[e]Refrence 4.

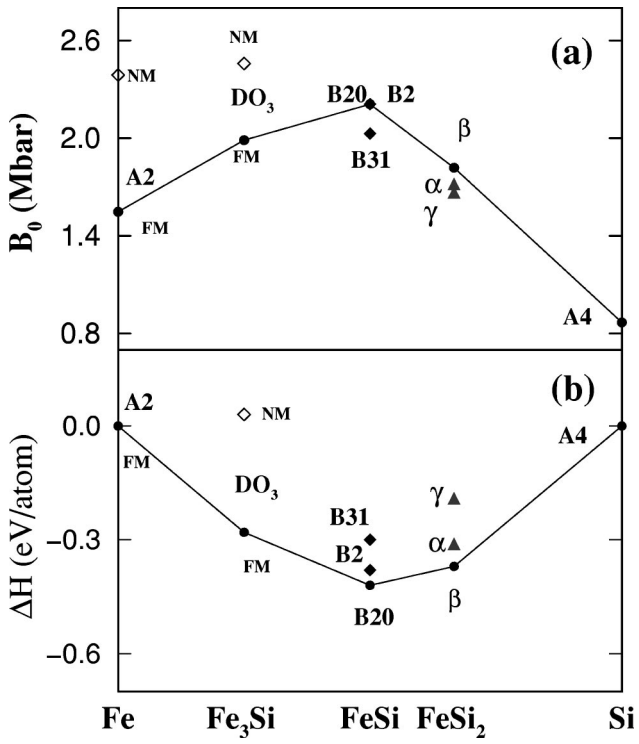

FIG. 4. Computed GGA cohesive properties for the Fe-Si compounds. (a) Equilibrium bulk modulus B_0 and (b) respective formation energy ΔH versus composition for stable and unstable structures. The bulk-stable structures are connected by a solid line.

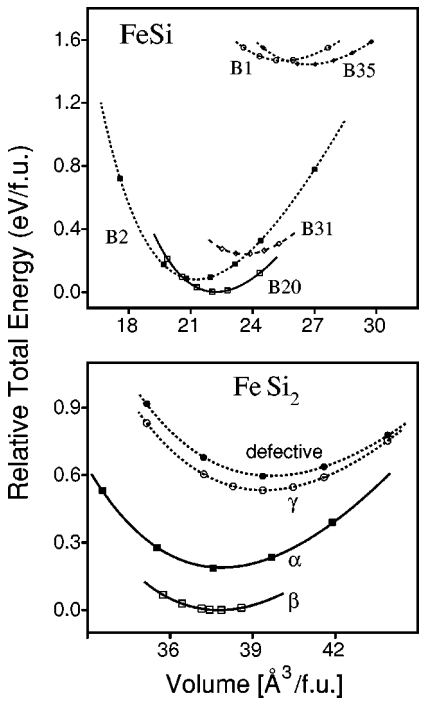

FIG. 5. Total energy curves versus equilibrium volume at the FeSi and $FeSi_2$ composition. The total energies of the bulk stable structures ($B20$ FeSi, β- and α-$FeSi_2$) are plotted as solid lines while the total energy of the unstable compounds (see respective structure symbol) are plotted using dashed or pointed lines.

silicides are in close agreement with the GGA results. Quite generally, compared to the LSD, the GGA leads to a reduced heat of formation ΔH and stabilizes the FM over the NM phases. This is most pronounced for Fe_3Si where the LSD predicts an exothermic ΔH for both the FM and NM phases whereas with the GGA the formation of a NM Fe_3Si compound is an endothermic process. Ferromagnetic order stabilizes the formation of the DO_3-type while for NM Fe_3Si the DO_3 structure is unstable with respect to tetragonal distortion.

As presented in Table III, GGA lattice constants are systematically larger than the LSD one and closer to experimental data. The relative changes between GGA and LSD V_0 results ($\Delta V/V$) vary from 10.1 to 3.5% going from pure Fe to Si. $\Delta V/V$ decreases linearly with increasing Si content but at a fixed composition does not depend on the type of structure. In Fe_3Si the LSD approximation underestimate at most the Fe-Si nearest-neighbor and second nearest-neighbor distances, which are of 2.38 and of 2.74 Å, respectively, while the experimental values are of 2.45 and 2.83 Å. GGA corrects completely the LSD interatomic distances prediction.

Concerning the bulk modulus, the GGA values are lower with respect to the LSD results and $\Delta B/B$ changes from -52% in Fe to -8% in Si. Note, however, that all the B_0 values in Table III have been evaluated at the respective theoretical V_0, which are different for LSD and GGA. The agreement with experiment for the GGA bulk modulus is improved for Fe, Fe_3Si, and FeSi while it becomes worse for Si. The pressure derivative of the bulk modulus B_0' ranges between 3.9 and 4.3 for all studied systems.

LSD cohesive energies are typically overestimated by 2.19 eV/atom for Fe and by 0.70 eV/atom for Si. The GGA corrections to E_{coh} provides therefore excellent agreement only for Si. The remaining discrepancy in E_{coh} with experiment, of about 1.0, 0.7 and 0.5 eV/atom for Fe, Fe_3Si, and FeSi may be overcome by improving the calculation of the total energy of the Fe atom through the use of orbital dependent potentials.[34] Finally, this study shows that GGA total energy calculations provide the most realistic equilibrium properties for Fe-Si compounds not only for the bulk stable but also for the artificial $B2$ and $C1$ structures. Therefore, in the following section we will mainly present *ab initio* calculations obtained using USPP and the GGA functional.

B. FeSi monosilicides

1. Structural stability

Figure 5 presents the computed total energy versus volumes curves for the $B20$, $B2$, $B31$, $B35$, and $B1$ structures (listed here in the order of decreasing stability). At this stoichiometry all studied phases are NM and the $B20$ structure is the most stable in agreement with the experimental phase diagram. The energy difference with respect to the $B31$ and the $B2$ structures is very small, ranging from ≈ 0.1 to 0.3 eV per formula unit. The larger coordination of the Fe and Si atoms in the $B2$ structure with respect to $B20$ and $B31$ explains the variation of the equilibrium volume in sequence $V_{B2} < V_{B20} < V_{B31}$. The $B31$ structure becomes more stable than $B20$ for increased $3d$ valence-electron composition like for the NiSi compound,[46] while $B2$ FeSi under compressive strain is stabilized by coherent epitaxy on Si(111).

TABLE IV. Comparison between calculated and experimental structural properties of ϵ-FeSi. The equilibrium lattice constant a_0, the bulk modulus computed with and without atomic relaxations, B_0 and B_0^0, respectively, the internal atomic coordinate $u(X)$, X = Si,Fe , the transition pressure p, the relative volume change ΔV, and the total energy difference ΔE, between the bulk-stable $B20$ and the unstable $B2$ structure are computed using two different GGA USPP. For the Fe atom the GGA USPP $ps1$ was generated for the $4s^1 3d^7$ and $ps2$ for the $3p^6 4s^1 3d^7$ atomic configurations.

		FeSi		
		USPP		Exp.
		$ps1$	$ps2$	
a_0	Å	4.463	4.469	4.489 [a]
B_0^0	Mbar	2.23	2.24	
B_0	Mbar	2.09		1.1-1.3 [b]
u(Fe)		0.136	0.136	0.137 [a]
u(Si)		0.841	0.841	0.842 [a]
p_{B20-B2}	Mbar	0.13	0.15	
ΔV_{B20-B2}	%	4.29	4.35	
ΔE_{B20-B2}	eV/f.u.	0.07	0.09	

[a]Reference 36.
[b]Reference 43.

The $B20$ structure (ϵ-FeSi) is the ground-state structure and it consists of a simple cubic Bravais lattice with four Fe and four Si atoms with coordinates (u,u,u), $(0.5+u,0.5-u,-u)$, $(-u,0.5+u,0.5-u)$, and $(0.5-u,-u,0.5+u)$, where u(Fe)=0.1358, u(Si)=0.844, and the lattice parameter a=4.489 Å.[42] The Si atoms in the $B20$-type lattice are isolated and bonded to metal atoms only. This structure is very peculiar because for u(Fe)=0.150 and u(Si)=0.850 each Si (Fe) atoms would have exactly seven Fe (Si) nearest neighbors.

The computed GGA structural properties of $B20$ FeSi are presented in Table IV. The lattice constant a_0 and the internal relaxed atomic coordinate of Fe and Si atoms [u(X), X =Fe,Si] compare very well with experimental values,[42] while the computed bulk modulus B_0=2.09 Mbar, is nearly a factor two larger than the measured value of 1.3-1.1 Mbar.[43] The difference ΔB between the bulk modulus computed without (B_0^0) and with fully atomic relaxation (B_0) is of 0.15 Mbar. Finite temperature and spin-waves effects are not treated in our calculation. These effects may reduce by about 10-20 % the computed elastic constants, and therefore, we still cannot explain the large difference between the computed and the measured bulk modulus of $B20$ FeSi. This number is usually taken without criticism also by more recent experimental work[4] therefore, we find that because of the overall agreement of our calculations for other Fe-Si bulk properties, this motivates new measurements of the corresponding elastic properties.

Mattheiss and Hamann[11] have described the Fe and Si atomic positions in $B20$ FeSi in terms of pairing-type distortion from the rocksalt ($B1$) structure. For this type of deformation the Bravais lattice is still simple cubic, but the overall point symmetry is tetrahedral. Along this deformation path from the $B20$ to the $B1$ structure, the internal atomic coordinate parameters change continuosly from u(Fe)=0.1358, u(Si)=0.8440 in $B20$ to u(Fe)=0.25 and u(Si)=0.75 in $B1$, respectively. The corresponding deformation energy raises from 0.0 to 1.4 eV without any activation barrier and the equilibrium volume per f.u. increases linearly from 22.2 to 25.5 Å^3. Thus, this large total energy difference precludes any possible high-temperature stabilization of FeSi into the more symmetric $B1$ structure.

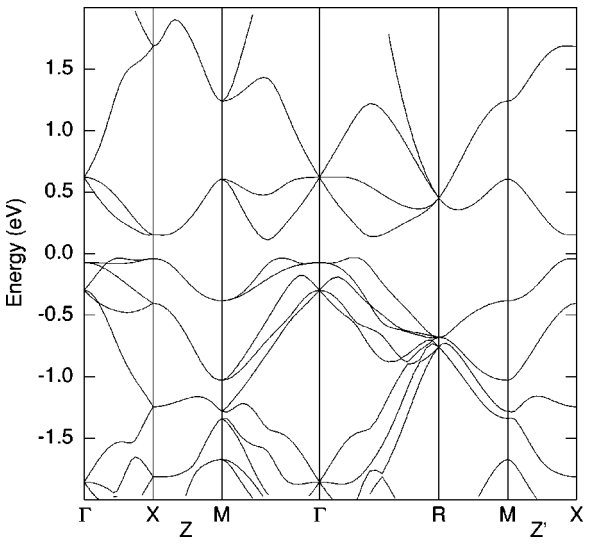

FIG. 6. USPP energy-band structure near the Fermi energy for ϵ-FeSi along symmetry lines in the simple cubic Brillouin zone.

2. ϵ-FeSi: *Electronic structure*

$B20$ FeSi is semiconducting according to both LDA and GGA calculations. The GGA band results near the Fermi level are plotted along symmetry lines in the simple cubic Brillouin zone in Fig. 6. We have plotted these bands using the same energy window as used by Mattheiss and Hammann in Fig. 3 of Ref. 11. Our band calculation is based on the GGA (ps1) equilibrium lattice parameter and atomic internal positions [u(Fe) and u(Si)] which are summarized in Table IV. The overall band topology for FeSi does not change by using the GGA exchange-correlation functionals, and the present bands are in excellent agreement with the LDA LAPW bands of Ref. 11. GGA predicts only slightly larger gaps but does not change the location of the indirect gap. The GGA calculated minimum gap is indirect (Δ_{ind}) and has a magnitude of about 0.15 eV, which is only slighty larger than the LDA value of 0.11 eV.[11] In agreement with LDA band calculations, Δ_{ind} involves the valence-band maximum along the ΓR line and the conduction-band minimum along ΓM. The minimum GGA band direct gap occurs along ΓM and is of about 0.18 eV, which however is only 0.01 eV smaller than the direct gap at X, Δ_X.

The pressure dependence of the computed indirect and direct gaps at selected high-symmetry points are listed in Table V. The isotropic pressure changes cause the modifications of the atom-position internal coordinates u(Fe) and u(Si) of about 0.04 and 0.02, respectively. However, these changes do not influence the magnitude and the location of the calculated indirect gap Δ_{ind} and direct gap Δ_X. At all studied pressures, the valence band near the Fermi energy is dominated by a rather flat $3d$ band along the ΓX direction while the first conduction band displays a more parabolic

TABLE V. Structural properties and band gaps of ϵ-FeSi at three different lattice constants a. The structural data such as the internal pressure p, the atomic relaxation energy gain ΔE_{rel}, and the corresponding atomic coordinate $u(X)$, X=Si,Fe are presented together with the the corresponding indirect Δ_{ind} and high-symmetry Δ_X, Δ_Γ, and Δ_R band gaps. For the indirect gap Δ_{ind} the direction in reciprocal space is given in parentheses.

		ϵ-FeSi		
a	Å	4.30	4.45	4.60
p	kbar	310	21	−153
ΔE_{rel}	meV/f.u.	8.7	0.0	8.5
u(Fe)		0.1398	0.1360	0.1302
u(Si)		0.8425	0.8408	0.8383
$\Delta_{ind}(\Gamma\text{-}R\rightarrow\Gamma\text{-}M)$	eV	0.147	0.148	0.159
Δ_X	eV	0.198	0.196	0.197
Δ_Γ	eV	0.844	0.705	0.590
Δ_R	eV	1.340	1.148	0.993

dispersion along the studied high-symmetry lines. A comparison of the theoretical band calculations at equilibrium lattice constant with the band topology provided recently by angle-resolved ultraviolet photoemission for bulk FeSi (100) (Ref. 44) and epitaxial FeSi (111) (Ref. 45) indicates a good agreement of the overall feature at room temperature, especially for the ΓR direction.

3. High-pressure B2 structure

The $B2$ equilibrium volume is smaller by about 4.5 % than the volume of the $B20$ ground-state structure. Because of the small structural energy difference a $B20$-$B2$ phase transition at a pressure of about 150 kbar is predicted. This two structures are connected continuously via the rocksalt structure ($B1$). FeSi displays a local minimum with the $B2$ structure and is unstable in the $B1$ structure. $B1$ FeSi may transform into the $B2$ structure following a Bain path along the [111] direction, but also may transform into the $B20$ structure by relaxing the internal atomic degree of freedom.[11]

The local stability of $B2$ FeSi is illustrated with respect to a tetragonal and trigonal Bain deformations in Fig. 7 for three different volumes: V_0, $0.8\times V_0$, and $1.2\times V_0$, where V_0 is its theoretical equilibrium volume. These transformation paths consist in the tetragonal distortions of the $B2$ lattice along the [001] axis, for the tetragonal deformation, and along the [111] axis, for the trigonal deformation. Along these paths, the crystal volume is constrained to be constant[47] and as shown in Fig. 7 the deformed structure can be parametrized in terms of the c/a ratio. Along the tetragonal Bain path, FeSi exhibits only a local minimum for the $B2$ structure ($c/a=1$) while along the trigonal path a second local minimum is found for $c/a=3.5$. The position of this second local minimum changes for different fixed volumes. Along the trigonal Bain path the hexagonal geometry is kept fixed, while the distances between the different (111) planes change together with the distance between the atoms in each plane. Along this path, the $B2$ ($c/a=1$) and the $B1$ ($c/a=2$) are the high-symmetry structure and are connected continuously.

Even if the total energy of the $B2$ and $B20$ structure are still close, the difference in local coordination of the $B2$ and

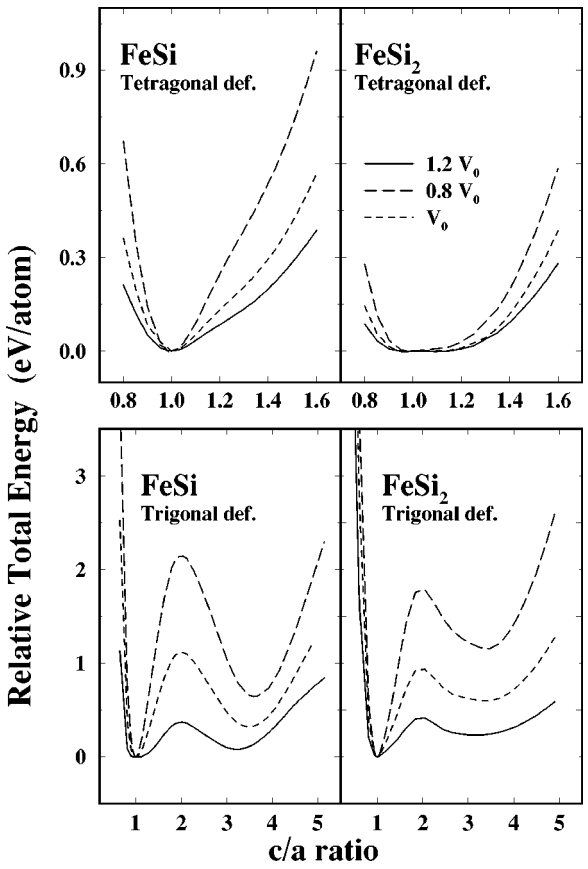

FIG. 7. Total energy versus c/a ratio at three very different constant volumes for FeSi and $FeSi_2$ along (a) the tetragonal and (b) the trigonal deformation path. $c/a=1$ denotes the $B2$ and CaF_2 structure, respectively.

$B20$ structure is strongly affecting the corresponding density of states. $B2$ FeSi is metallic and has a DOS that is bcc like (see Fig. 8) dominated by a 2 eV narrow peak of the metal $3d$ bands while the DOS of $B20$ FeSi is more fcc like without a dominating peak and displays a small gap. For $B2$ FeSi the Fermi level falls near a pseudogap of the density of states at the onset of a sharp peak of Fe d states and separates the occupied bonding states from the empty states. These differences in electronic properties of $B20$ and $B2$ FeSi illustrate how also other related properties of the materials may change during a $B20$-$B2$ structural change.

C. $FeSi_2$ disilicides

1. Structural stability

Figure 5(b) describes the computed total energy curves versus volume for various stable (β,α) and unstable (γ and defected) crystal structures of $FeSi_2$. Compared to previous results from a semiempirical tight-binding approach[48] qualitative agreement on the structural stability hierarchy is observed. The destabilization of the γ- with respect to the β-phase by 0.54 eV/f.u. using GGA (or 0.51 eV using LDA) compares quite well with about 0.49 eV/f.u. found by semiempirical methods.[48] The structural energy difference between α- and β-phase of 0.04 eV/f.u. predicted by semiempirical methods[48] is, however, underestimated by a factor of about four when compared to the first-principles result of

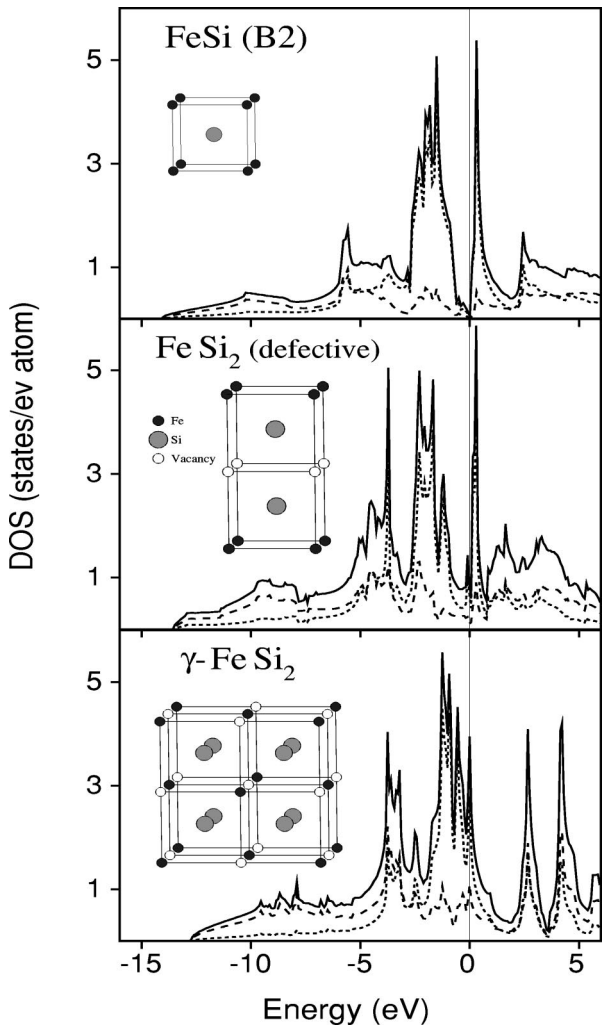

FIG. 8. Unit cells and density of states for (a) $B2$-FeSi and two defective CsCl-based structures, (b) related to the α-, and (c) identical with the γ-phase.

0.15 eV/f.u. using LDA or 0.18 eV/f.u. using GGA. This comparison reflects a poor transferability of tight-binding parameters (fitted using the bands of the cubic $B2$ FeSi and γ-$FeSi_2$) for the tetragonal α-structure, which shows very strong Si-Si contacts.

The ground-state of $FeSi_2$ is the semiconducting orthorhombic β structure, which has been described by Dusausoy *et al.*[40] The β structure in its primitive cell contains eight formula units for the base-centered structure and deviates from the γ-$FeSi_2$ only through small deformation and rotations of the cubic cages in the fluorite structure.

The structural properties of β-$FeSi_2$ using GGA calculations compare well with the experimental results. The computed theoretical GGA lattice parameters of the orthorhombic cell are $a=9.901$, $b=7.779$, and $c=7.833$ Å and compare well with the corresponding experimental values of $a=9.863$, $b=7.791$, and $c=7.833$ Å.[40] The agreement with experimental observation for the Fe-Si, Fe-Fe, and Si-Si distances is also very good. The computed and experimental Fe-Fe, Fe-Si, and Si-Si bond lengths differ at maximum of about 0.02 Å.

When the progressive distortion of the atomic positions is generated by a linear interpolation between the atomic positions and cell dimensions of the γ and β structures and represented by a configurational parameter ϵ ranging from 0 to 1, respectively, the band-gap opening is only produced in the vicinity of the β phase for $\epsilon>0.8$. Along this distortion path the systems decrease its total energy without passing through a barrier, as is expected for a Jahn-Teller-like symmetry splitting of bands and is mainly characterized by a reduction of the corresponding Fe-Fe and Si-Si interatomic distances, of about 0.8 and 0.1-0.3 Å, respectively. The shortening of the Fe-Fe distance and the deformation of the Si cages surrounding the eight-folded coordinated Fe atoms, passing from the cubic structure to a solid with two square faces and four nearly regular trapezoidal faces, give rise to the formation of the band gap also for the local electronic DOS of the Fe atoms. The metallic-semiconductor displacive transition in $FeSi_2$ is correlated with these Jahn-Teller distortions which occur at selected sites in different times,[20] and involve locally these eightfold cages of Si atoms with Fe inside.

2. β-$FeSi_2$: *Electronic structure*

A semiconducting gap of $0.84-0.87$ eV has been detected,[49] however despite a lot of experimental efforts, there is still no agreement about the characteristics and the nature of the band gap in β-$FeSi_2$. The gap properties of the β-$FeSi_2$ ordered compound have been initially investigated by Eppenga[16] using the augmented spherical wave method and Christensen[15] who employed the linear muffin-tin orbital (LMTO) method. Both authors claimed an indirect gap, but they disagree on the identification of the gap transition and on the width that is calculated within a range of 0.44 up to 0.80 eV. In these first studies[15,16] it was also shown that the calculated gap depends on the ratio r of the atomic sphere radii of Fe and Si. This shows immediately that these methods are not reliable for these quantities. A detailed comparison between gap properties and their relation to the choice of r for the LMTO method is discussed in Ref. 50.

Compared to other first-principle results[15–17,51] the FLAPW and USPP calculations in the vicinity of the band gap plotted in Fig. 9 reveal a surprisingly different topology of the bands close to the gap. The valence-band edge is not located in the region between Γ and Z $(=\Lambda)$ as in Refs. 16 and 51 but at the symmetry point Y of the Brillouin zone of the orthorhombic centered cell. The indirect nature of the fundamental gap is therefore confirmed but attributed now to a transition with an energy of 0.58 eV between Y and 0.6 $\times\Lambda$. The direct transition with an energy of 0.06 eV higher than the indirect one (0.64 eV) is located at Y. By using GGA, the magnitude of the gaps is increased by 0.04 eV, but they do not affect the topology of the LDA bands shown in Fig. 9. Compared to experimental data the computed direct and indirect gap are 30% too small. This discrepancy is within the range usually observed for density-functional results on band-gap energies.

Very recently,[52] a pseudopotential study applying GGA was performed resulting in a very similar topology of the electronic structure at the gap. Similar to our findings an indirect Y-Λ gap was found. However, the gap sizes reported by Clark *et al.*[52] are larger, e.g., 0.73 eV (compared to 0.62 eV for our GGA calculation) for the indirect gap. This difference might be due to the slightly different lattice parameters derived for the bulk ground state: our data for a and b

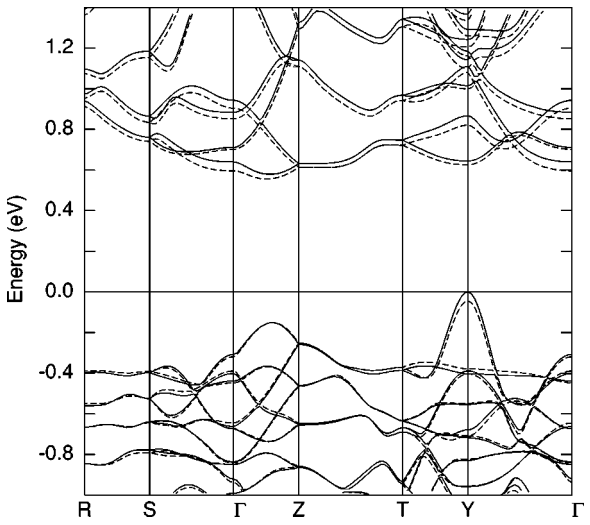

FIG. 9. Band structure near the Fermi energy for β-$FeSi_2$ along symmetry lines in the orthorombic-centered Brillouin zone. Comparison between FLAPW energy-band results (solid lines) and USPP band structure (dashed lines).

are larger (within 1%) whereas the c parameter is smaller by $\approx 1\%$ than the corresponding values of Ref. 52.

The disagreement between methods applying spherical and full potential basis functions on the band topology near the gap in the vicinity of Y can be understood by an inspection of the partial charges of the state at Y given in Table VI. The highest occupation state turns out to be highly delocalized with 54% of the charge in the interstitial region. The delocalizations accounts also for the relatively strong dispersion of the corresponding band. It is therefore not at all surprising that this band may be better represented by full potential basis functions. Additional to the high interstitial partial charge a pronounced p character (more than d) is observed. This is especially important for estimating the forbidden or allowed character of both, the indirect and direct across-gap transitions. Since the initial state exhibits considerable p character and both final states are quite localized Fe d states, the indirect and direct gap are therefore definitively not dipole forbidden. For those states that were considered as initial states for the gap transitions by previous calculations, i.e., Γ, Z, and $0.6\times\Lambda$, a comparable high Fe d character (see Table VI) prevented a definitive statement about the allowed character of the gap transitions. This study confirms the indirect nature of the fundamental gap and that the application of a full-potential method is necessary to study the band structure of β-$FeSi_2$.

TABLE VI. Partial charges (%) of the states around the gap at the Y-, $0.6\times\Lambda$-, Γ-, and Z point. The energies are given relative to the Fermi energy E_F. The two different rows of data per band give results for the two inequivalent Fe and Si atoms. The muffin-tin radii of Fe and Si atoms are $r_{MT}=1.11$ Å and INT denotes the interstitial region.

	Band	Energy		Fe			Si		
State	no.	[eV]	s	p	d	s	p	d	INT
Y	64	0.0	0.1	4.6	2.7	0.3	7.2	3.8	53.9
			0.7	6.5	9.2	0.0	7.6	3.4	
		gap							
	65	0.644	0.4	0.4	21.1	0.6	1.7	1.8	8.3
			0.0	0.1	59.4	4.6	1.0	0.6	
0.6Λ	64	−0.152	0.0	0.2	25.1	0.3	4.8	1.4	25.4
			0.1	2.3	34.8	0.1	3.4	2.1	
		gap							
	65	0.579	0.0	0.3	47.8	0.1	2.3	0.6	12.0
			0.0	0.4	32.3	1.3	2.7	0.2	
Γ	64	−0.308	0.0	4.6	6.3	0.1	12.2	2.1	29.2
			0.0	1.7	39.9	0.0	2.1	1.8	
		gap							
	65	0.640	0.0	1.2	45.5	0.5	2.6	1.2	14.9
			0.0	0.2	24.4	2.7	6.4	0.4	
Z	64	−0.258	0.1	1.4	29.8	0.3	2.7	1.3	19.7
			0.3	1.9	38.1	0.1	2.5	1.8	
		gap							
	65	0.632	0.0	0.3	41.3	1.1	4.1	1.1	14.9
			0.0	0.7	31.7	0.7	3.8	0.3	

3. α-$FeSi_2$: *High-temperature structure*

A second stable crystalline phase at the disilicide composition is α-$FeSi_2$. This phase is stable only above 920° C, is metallic and its crystal structure type is tetragonal with 3 atoms per unit cell, and lattice parameters of $a=2.690$ and $c=5.134$ Å. The α phase exist in the composition range 69 to 72.5 at. % silicon. The deviation from the stoichiometric composition is due to iron vacancies. This structure is characterized by uniplanar iron based layers with Si forming adjacent pairs, with as peculiar feature the directional bonding of Si atoms induced by the short Si-Si distance. The agreement between the computed GGA and experimental lattice parameters is very good, confirming the very small Si-Si nearest neighbor (NN) distance of 2.33 Å when compared to the Fe-Fe NN distance of 2.71 Å. Taking into account all possible relaxations the α-structure is higher in energy with respect to the β-phase by 0.15 eV in the LSD and by 0.19 eV in the GGA.

The structural properties of α-$FeSi_2$ are presented in Table II. The calculations lead to similar structural properties independently from the used functional. Compared to experiment the main difference occurs for the internal Si atomic coordinates z_i. This disagreement results in an increase of about 0.1 Å of the Si-Si NN distance and is probably connected to the presence of Fe vacancies in the experimental sample, which are not considered here. The relaxation of z_i from the experimental value 0.28 to 0.273 lowers E_{tot} of 0.05 eV and is related to the shift of the Fe $3d$ and Si $3p$ DOS of ≈ 0.2 eV at lower energy. The Fermi level of α-$FeSi_2$ is located in a pronounced minimum (see Fig. 3) which reduces the band structure energy and explains its relative stability with respect to the unstable $C1$ structure.

4. γ-$FeSi_2$ *and related structures*

The $FeSi_2$ pseudomorphic structures appearing at the interface to silicon have been interpreted, from a geometrical point of view, as $B2$ based lattices with random arrangements of vacancies on the Fe sublattice,[4] because the sym-

metry of these phases does not change during the annealing process. Assuming that each vacancy should have the maximum number of nearest neighbor vacancies compatible with the disilicide stoichiometry leads to the formation of (001) layers of vacancies. As a consequence the cubic symmetry is reduced to a tetragonal one with $c=2a$. After relaxation of the c lattice parameter and of the silicon atomic positions the α-$FeSi_2$ is formed. On the other hand, the γ-$FeSi_2$ emerges from the requirement that all vacancies should have the maximum number of next-nearest neighbors. In this structure each Si atom is tetrahedrally coordinated with four Fe atoms and each Fe atom has eight Si nearest neighbors.

Experimentally, these defected cubic phases have been observed as intermediate precursor phases of the stable β-$FeSi_2$ phases during silicide heteroepitaxy on Si substrates. The metallic α-$FeSi_2$ has been stabilized[53] in epitaxially grown layers at temperatures far below its stability range in the bulk phase, while γ-$FeSi_2$ has been formed in very thin films[54,55] by annealing 3-7-Å thick Fe films deposited on Si(111) between 250 and 550 °C.

As for the monosilicides, also for the disilicide series with $C1$ structure the rigid band-assumption is nearly fulfilled and a ''quasigap'' in the DOS near E_F at the $CoSi_2$ band filling separates bonding and antibonding states. The bonding properties of $FeSi_2$ are understood in terms of hybridization of d-metal and p-silicon states.[19] The covalent bonding stabilizes the $C1$ structure for $CoSi_2$ and $NiSi_2$ but is not sufficient for $FeSi_2$ (Ref. 15) because here the Fermi level is located in a giant peak of Fe states mixed with Si p states [see Fig. 8(c)], indicating that the $C1$ structure is highly unstable.

The total energy of the tetragonal defected $FeSi_2$($c=2a$, $z_i=0.25$) and of γ-$FeSi_2$ are shown in Fig. 5(b). In agreement with experiment we found that both studied $FeSi_2$ defected structures are unfavorable situation as bulk structures. By constraining γ-$FeSi_2$ to volumes larger than the equilibrium volume, a ferromagnetic moment develops on Fe atoms. For lattice constants of 5.7, 5.6, and 5.5 Å, the Fe magnetic moment (M_{Fe}) are of 0.78, 0.52, and 0.42 μ_B, respectively. At the equilibrium lattice constant of $a_0=5.4$ Å M_{Fe} drops to zero. These calculation do not indicate a magnetic stabilization of the fluorite phase, however they reveal the possibility of obtaining a ferromagnetic Fe sublattice by stabilizing the fluorite structure at large volume. The control of the magnetic properties of the γ-$FeSi_2$, together with the properties of defected FeSi $B2$ compounds are peculiar for the design of Fe/$FeSi_2$ or FeSi/Fe_3Si multilayers.

γ-$FeSi_2$ and the tetragonal defected $FeSi_2$ are also mechanical unstable with respect to tetragonal or local deformations. The defected tetragonal structure relaxes towards the stable α-$FeSi_2$ while the γ-$FeSi_2$ evolve towards the β-$FeSi_2$. One peculiar feature of γ-$FeSi_2$ is its local stability along the trigonal Bain deformation as shown in Fig. 7. However, γ-$FeSi_2$ differently from the $B2$ FeSi shows a clear instability along the tetragonal Bain path, which is mostly related to the tetragonal instability of the fcc Fe sublattice. This fact reflects the experimental finding that γ-$FeSi_2$ may be epitaxially stabilized on Si(111) while there is no evidence of stabilization of the γ-$FeSi_2$ on Si(100) substrate.

IV. CONCLUSION

We studied the cohesive, electronic, and structural properties of several Fe-Si compounds by using GGA and an ultrasoft pseudopotential approach as well as a full potential all-electron method. For structural properties GGA improves substantially the agreement with experiment as compared to LDA results. The relative stability of the studied phases is however not affected by the choice of functional. At the 1:1 and 1:2 composition, the Fe-Si compounds display a very rich structural phase diagram with several metastable cubic structures which may be stabilized by high pressures or by epitaxial growth. In contrast to the β-$FeSi_2$ and ϵ-FeSi ground-states bulk phases, which are semiconductors, these pseudomorphic cubic phases are metallic conductors. The structural transition from the semiconducting to the metallic phases are characterized by changes of the local atomic coordination as also expressed in the corresponding density of states. The calculated configurational magnetic effects in Fe_3Si and the semiconductive properties of β-$FeSi_2$ and ϵ-FeSi compounds and the derived bands indicate the importance of using precise *ab initio* methods, which make no shape approximation to the one-electron potential.

Finally, our study demonstrates the accuracy of USPP for describing not only the electronic, magnetic, and structural properties of stable phases but also for the calculation of properties of related unstable structures over a wide pressure range. Based on *ab initio* results for artificial bulk structures the continuous progress in the field of epitaxial growth opens the possibility to design new Fe-Si multilayer materials with very high-crystalline quality and very peculiar optical or magnetic properties.

ACKNOWLEDGMENTS

This work was supported by the Center of Computational Materials Science (CMS) in Vienna. One of us (E.G.M.) acknowledges support by the Swiss National Science Foundation under Grant No. 8220-042840. Partial support was given by the City of Vienna under Grant No. H-00106/96.

[1] G. W. Rubloff, Surf. Sci. **132**, 268 (1983); S. P. Murarka and M. C. Peckerar, in *Electronic Materials, Science and Technology*, edited by J. Streichen (Academic, Boston, 1989), p. 267; H. Lange, Phys. Status Solidi B **101**, 3 (1997).

[2] S. Saitoh, H. Ishiwara, T. Asano, S. Furukawa, Jpn. J. Appl. Phys., Part 1 **20**, 1649 (1981); R. T. Tung, J. M. Gibson, J. M. Poate, Phys. Rev. Lett. **50**, 429 (1983).

[3] N. Cherief, C. D'Anterroches, R. C. Cinti, T. A. Nguyen Tan, and J. Derrien, Appl. Phys. Lett. **55**, 1671 (1989); A. Rizzi , B. N. E. Rösen, D. Freundt, Ch. Dieker, H. Lüth, and D. Gerthsen, Phys. Rev. B **51**, 17 780 (1995).

[4] H. von Känel, K. A. Mäder, E. Müller, N. Onda, and H. Sirringhaus, Phys. Rev. B **45**, 13 807 (1992); H. von Känel, M. Mendrik, K. A. Mäder, N. Onda, S. Goncalves-Conto, C. Schwarz, G. Malegori, L. Miglio, and F. Marabelli, **50**, 3570 (1994); H. von Känel, E Müller, S. Goncalves-Conto, C. Schwarz, and N. Onda, Appl. Surf. Sci. **104/105**, 204 (1996).

[5] J. E. Mattson, S. Kumar, E. E. Fullerton, S. R. Lee, C. H. Sowers,

M. Grimsditch, S. D. Bader, and F. T. Parker, Phys. Rev. Lett. **71**, 185 (1993); K. Inomata, K. Yusu, and Y. Saito, *ibid.* **74**, 1863 (1995).

[6] J. Kohlhepp, M. Valkier, A. van der Graaf, and F. J. A. Den Broeder, Phys. Rev. B **55**, R696 (1997); S. Toscano, B. Briner, H. Hopster, and M. Landolt, J. Magn. Magn. Mater. **114**, L6 (1992); E. Fullerton, J. E. Mattson, S. R. Lee, C. H. Sowers, Y. Y. Huang, G. Felcher, S. D. Bader, and F. T. Parker, *ibid.* **117**, L301 (1992).

[7] R. Kläsges, C. Carbone, W. Eberhardt, C. Pampuch, O. Rader, T. Kachel, and W. Gudat, Phys. Rev. B **56**, 10 801 (1997).

[8] J. Kudrnovsky, N. E. Christensen, and O. K. Andersen, Phys. Rev. B **43**, 5924 (1991).

[9] V. A. Niculescu, T. J. Burch, and J. I. Budnick, J. Magn. Magn. Mater. **39**, 223 (1983).

[10] H. Busse, J. Kandler, B. Eltester, K. Wandelt, G. R. Castro, J. J. Hinarejos, P. Segovia, J. Chrost, E. G. Michel, and R. Miranda Surf. Sci. **381**, 133 (1997).

[11] L. F. Mattheiss and D. R. Hamann, Phys. Rev. B **47**, 13 114 (1993).

[12] T. Jarlborg, Rep. Prog. Phys. **60**, 1305 (1997); Phys. Rev. B **51**, 11 106 (1995).

[13] D. Mandrus, J. L. Sarrao, A. Migliori, J. D. Thompson, and Z. Fisk, Phys. Rev. B **51**, 4763 (1995).

[14] C. Fu, M. Krijnh, and S. Doniach, Phys. Rev. B **49**, 2219 (1994).

[15] N. E. Christensen, Phys. Rev. B **42**, 7148 (1990).

[16] R. Eppenga, J. Appl. Phys. **68**, 3027 (1990).

[17] V. N. Antonov, O. Jepsen, W. Henrion, M. Rebien, P. Strauss, and H. Lange, Phys. Rev. B **57**, 8934 (1998).

[18] S. Eisebitt, J.-E. Rubensson, M. Nicodemus, T. Böske, S. Blügel, W. Eberhardt, K. Radermacher, S. Mantl, and G. Bihlmayer, Phys. Rev. B **50**, 18 330 (1994).

[19] K. A. Mäder, H. von Känel, and A. Baldereschi, Phys. Rev. B **48**, 4364 (1993).

[20] L. Miglio, V. Meregalli, F. Tavazza, and M. Celino, Europhys. Lett. **37**, 415 (1997).

[21] E. G. Moroni *et al.* (unpublished).

[22] G. Kresse and J. Furthmüller, Comput. Mater. Sci. **6**, 15 (1996); Phys. Rev. B **54**, 11 169 (1996).

[23] J. Perdew and A. Zunger, Phys. Rev. B **23**, 5048 (1981).

[24] J. P. Perdew and Y. Wang, Phys. Rev. B **45**, 13 244 (1992), and references therein.

[25] U. von Barth and L. Hedin, J. Phys. C **5**, 1629 (1972).

[26] J. A. White and D. M. Bird, Phys. Rev. B **50**, 4954 (1994).

[27] D. M. Wood and A. Zunger, J. Phys. A **18**, 1343 (1985).

[28] H. Jansen and A. J. Freeman, Phys. Rev. B **30**, 561 (1984); E. Wimmer, H. Krakauer, M. Weinert, and A. J. Freeman, *ibid.* **24**, 864 (1981).

[29] H. J. Monkhorst and J. D. Pack, Phys. Rev. B **13**, 5188 (1976).

[30] P. E. Blöchl, O. Jepsen, and O. K. Andersen, Phys. Rev. B **49**, 16 223 (1994).

[31] N. D. Mermin, Phys. Rev. **137**, A1141 (1965).

[32] A. T. Paxton, M. Methfessel, and H. M. Polatoglou, Phys. Rev. B **41**, 8127 (1990).

[33] D. Vanderbilt, Phys. Rev. B **41**, 7892 (1990); K. Laasonen, A. Pasquarello, R. Car, Ch. Lee, and D. Vanderbilt, *ibid.* **47**, 10 142 (1993).

[34] E. G. Moroni, G. Kresse, J. Hafner, and J. Furthmüller, Phys. Rev. B **56**, 15 629 (1997); G. Kresse and J. Hafner, J. Phys.: Condens. Matter **6**, 8245 (1994).

[35] S. G. Louie, S. Froyen, and M. L. Cohen, Phys. Rev. B **26**, 1738 (1982).

[36] P. Villars and L. D. Calvert, *Pearson's Handbook of Crystallographic Data for Intermetallic Phases* (American Society for Metals, Materials Park, OH, 1985).

[37] C. Kittel, *Introduction to Solid State Physics*, 6th ed. (Wiley, New York, 1986).

[38] F. D. Murnaghan, Proc. Natl. Acad. Sci. USA **30**, 244 (1944); F. Birch, J. Geophys. Res. **57**, 227 (1952).

[39] A. R. Williams, V. L. Moruzzi, C. D. Gelatt, J. Kübler, and K. Schwarz, J. Appl. Phys. **53**, 2019 (1982).

[40] Y. Dusausoy, J. Protas, R. Wendji, and B. Roques, Acta Crystallogr., Sect. B: Struct. Crystallogr. Cryst. Chem. **B27**, 1209 (1971).

[41] F. R. de Boer *et al.*, in *Cohesion in Metals*, edited by F. R. de Boer and D. G. Pettifor (North-Holland, Amsterdam, 1988), Vol. 1.

[42] L. Pauling and A. M. Soldate, Acta Crystallogr. **1**, 212 (1948); H. Watanabe, H. Yamamoto, and K. Ito, J. Phys. Soc. Jpn. **18**, 995 (1963).

[43] G. P. Zinoveva, L. P. Andreeva, and P. V. Geld, Phys. Status Solidi A **23**, 711 (1974).

[44] G. R. Castro, J. Alvarez, M. E. Dávila, M. C. Asensio, and E. G. Michel, J. Phys.: Condens. Matter **9**, 1871 (1997).

[45] J. J. Hinarejos, P. Segovia, J. Alvarez, G. R. Castro, E. G. Michel, and R. Miranda, Phys. Rev. B **57**, 1414 (1998).

[46] E. G. Moroni (unpublished).

[47] E. C. Bain, Trans. Am. Inst. Min. Metall. Pet. Eng. **70**, 25 (1924); P. J. Craievich, J. M. Sanchez, R. E. Watson, and M. Weinert, Phys. Rev. B **55**, 787 (1997); Phys. Rev. Lett. **72**, 3076 (1994).

[48] L. Miglio, F. Tavazza, and G. Malegori, Appl. Phys. Lett. **67**, 2293 (1995); L. Miglio and G. Malegori, Phys. Rev. B **52**, 1448 (1995).

[49] M. C. Bost and J. E. Mahan, J. Appl. Phys. **58**, 2696 (1985); C. Giannini, S. Lagomarsino, F. Scarinci, and P. Castrucci, Phys. Rev. B **45**, 8822 (1992).

[50] W. Wolf, Ph.D. dissertation, Universität Wien, 1996.

[51] A. B. Filonov, D. B. Migas, V. L. Shaposhnikov, N. N. Dorozhkin, G. V. Petrov, V. E. Borisenko, W. Henrion, and H. Lange, J. Appl. Phys. **79**, 7708 (1996).

[52] S. J. Clark, H. M. Al-Allak, S. Brand, and R. A. Abram, Phys. Rev. B **58**, 10 389 (1998).

[53] J. Chevrier, P. Stocker, Le Thanh Vinh, J. M. Gay, and J. Derrien, Europhys. Lett. **22**, 449 (1993).

[54] N. Onda, J. Henz, E. Müller, K. A. Mäder, and H. von Känel, Appl. Surf. Sci. **56-58**, 421 (1992).

[55] X. Wallart, J. P. Nys, O. Dehaese, and G. Vincent, Appl. Surf. Sci. **70-71**, 598 (1993); X. Wallart, J. P. Nys, and C. Tetelin, Phys. Rev. B **49**, 5714 (1994).